JES Focus Issue on Lithium–Sulfur Batteries: Materials, Mechanisms, Modeling, and Applications

Self-Discharge Effects in Lithium-Sulfur Equivalent Circuit Networks for State Estimation

S. E. A. Yousif, A. Fotouhi, D. J. Auger,[z] and K. Propp

School of Aerospace, Transport and Manufacturing, Cranfield University, Cranfield, Bedfordshire MK43 0AL, United Kingdom

This study considers application-oriented models of lithium-sulfur (Li-S) cells. Existing ECN models often neglect self-discharge, but this can be important in applications. After describing the context in which control-oriented models and estimators are based, the self-discharge phenomenon is investigated for a new 21 Ah Li-S cell. As a contribution of this study, an equivalent-circuit-network (ECN) model was extended to account for cells' self-discharge. Formal system identification techniques were used to parameterize a model from experimental data. The original model was then extended by adding terms to represent a self-discharge resistance. To obtain the self-discharge resistance, a particular new series of experiments were designed and performed on the Li-S cell at various temperature and initial state-of-charge (SoC) levels. The results demonstrate the dependency of self-discharge rate on the SoC and temperature. The self-discharge rate is much higher at high SoC levels and it increases as temperature decreases.
© The Author(s) 2017. Published by ECS. This is an open access article distributed under the terms of the Creative Commons Attribution 4.0 License (CC BY, http://creativecommons.org/licenses/by/4.0/), which permits unrestricted reuse of the work in any medium, provided the original work is properly cited. [DOI: 10.1149/2.0121801jes] All rights reserved.

Manuscript submitted August 21, 2017; revised manuscript received November 2, 2017. Published November 30, 2017. *This paper is part of the JES Focus Issue on Lithium-Sulfur Batteries: Materials, Mechanisms, Modeling, and Applications.*

Much of today's research into lithium-sulfur (Li-S) batteries concerns the development and understanding of materials, construction and the fundamental scientific understanding of cell behavior. Many will recognize the importance of this, but lithium-sulfur is beginning to reach maturity, and there is a need to develop the engineering science and techniques necessary for deployment in practical applications. In particular, there is a need to devise algorithms that can be used to estimate state-of-charge and state-of-health measures *in operando*. Electrochemistry is of course key here, but it is equally vital to draw from other disciplines: in particular, control theory has much to offer, particularly in respect of state estimation.

When electrochemists create models, they usually do so 'as scientists': the aim of a scientific model is to enhance understanding. Of course, no model is perfect, and the pure scientist uses model imperfections to identify gaps in present knowledge and as the inspiration for further research. The aim is to improve understanding and get a 'better model'. However, at some point, cells may be put to practical use, and at this point, the application engineer will often have to make do with the best models available at that time, despite the model's imperfections.

Control systems engineers are well accustomed to dealing with model errors and 'uncertainty': there are many excellent text books on control, and any of them will give a short overview of the key principles of control; Aström and Murray's work[1] is a good example. Typically, a dynamic system is modelled as a set of dynamic equations:

$$\begin{aligned} y &= h\left(\Delta, x, u, v, w\right) \\ \dot{x} &= f\left(\Delta, x, u, w\right) \end{aligned} \qquad [1]$$

where u and y represent observed system input and outputs (voltages, currents and temperatures, for example), x comprehensively accounts for past history by representing the system's non- or partly-measurable dynamic 'states' (perhaps including state of charge in a simple model, or concentrations of chemical species in a complex one), $h(\cdot)$ and $f(\cdot)$ are known functions describing the system's nominal (or assumed) dynamic behavior. The remaining quantities represent 'unknowns': Δ represents the uncertain (and unknown) dynamics within the system; v represents 'observation noise' – perturbations to the measured output variables that cause our observations to differ from reality; w represents 'disturbances' – unmeasured external factors than nevertheless affect system behavior. Exactly how the uncertainty is modelled can depend somewhat on the control paradigm in use: sometimes, Δ is not explicitly used, and w is used to represent both the unknown dynamics and the external disturbances together. However, the key thing is that methods from control theory explicitly allow for modelling errors and uncertainty. The motivation for feedback control is to deal with this uncertainty and mitigate its effects.[2]

A substantial body of state estimation theory has been developed as part of control: the 'state space' methods and their derivatives such as the linear quadratic regulator[1] use control laws that depend on a measurement of the internal system state. When direct measurements are not available, it is necessary to estimate the internal state x. Estimation theory emerges as the 'dual' of state feedback control. The first step in the algorithm is to estimate the state at the current observation time using our model, the current input and the last state estimate:

$$\dot{x}_{\text{pred}}\left(t\right) = \hat{f}\left(x_{\text{est}}\left(t\right), u\left(t\right)\right) \qquad [2]$$

where x_{est} is the current state estimate, the function $\hat{f}(x,u) = f(0,x,u,0)$ represents the nominal (or assumed) model dynamics and t is the time of the current observation. The next step is to work out the 'prediction error' as a consequence of this:

$$\varepsilon_{\text{pred}}\left(t\right) = y\left(t_i\right) - \hat{h}\left(x_{\text{pred}}\left(\text{t}\right), u\left(t\right)\right) \qquad [3]$$

where $\varepsilon_{\text{pred}}$ is the prediction error and the function $\hat{h}(x,u) = h(0,x,u,0,0)$ again represents the assumed model behavior. The state estimate may then be calculated from

$$\dot{x}_{\text{est}}\left(t\right) = \dot{x}_{\text{pred}}\left(t\right) + k\left(\varepsilon_{\text{pred}}\left(t\right)\right) \qquad [4]$$

where $k(\cdot)$ is a 'correction' function, details of which will depend on the precise details of the algorithm used. Essentially, the idea of control-oriented state estimation is that if the estimate contains an error term, then this will result in a prediction error: this will result in a 'correction' to the internal state. Depending on the system dynamics and how the correction is designed, it is often possible to guarantee that the state estimate will converge to the true estimate.

It is beyond the scope of this paper to go into the detailed derivation of estimators: perhaps the best known are the Kalman filter family, initiated by Rudolph Kalman's seminal work.[3] This has been successfully applied to lithium-ion batteries by many authors, notably Plett.[4–6]

These techniques have recently been applied to lithium-sulfur for the first time. In this example, equivalent circuit network models were employed. Equivalent circuit network models will be described in

[z]E-mail: d.j.auger@cranfield.ac.uk

Downloaded on 2018-01-22 to IP 138.250.27.251 address. Redistribution subject to ECS terms of use (see ecsdl.org/site/terms_use) unless CC License in place (see abstract).

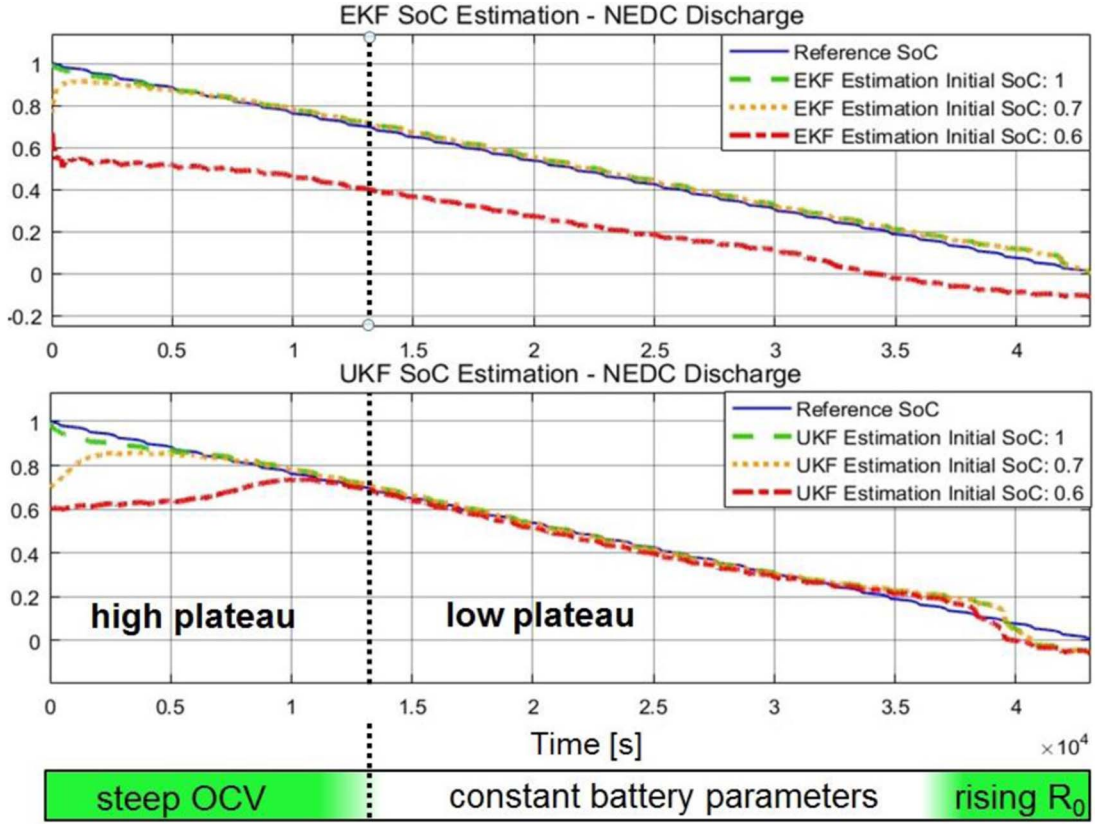


Figure 1. The Extended Kalman Filter (EKF) and Unscented Kalman Filter (UKF) have been demonstrated for use on real lithium-sulfur cells subject to automotive drive cycles: the UKF was found to cope better with unknown initial states of charge.[8]

more detail in ECN modelling approach section, but it is worth noting that their original application to lithium sulfur was carried out in works such as.[7–10] These were then used for state estimation in Ref. 11 The results for one such test are shown in Figure 1: in this test, two Kalman filter derivatives were applied to real Li-S cells subject to electrical demands representing automotive driving cycles, and – subject to certain limitations – were found to give a useful prediction of state of charge, in spite of the simplicity of the underlying models.

Closely related to these is a set of techniques from artificial intelligence based on Adaptive Neuro-Fuzzy Inference Systems (ANFIS).[12] While it should be very clear to the reader that an equivalent circuit network model is likely to be in some ways a gross over-simplification, what these works demonstrate is that even a fairly 'rough and ready' model can be used.

State estimation developments are expected to take into account improvements in the state of the art for executable models. A 'zero dimensional' electrochemical model for Li-S has recently been published[13] and while there is further work to be done to extend this and parameterize real, physical cells, this is a promising direction for future exploitation. As the state of the art in modelling develops, it is envisaged that it will be possible to explore state-of-the-art techniques for rapid online execution of spatially distributed models.[15] A possible road map is shown in Figure 2 including contributions by control engineers follow developments in fast-executing electrochemical models.

At present, however, we are still reliant on ECN models for state estimation, and the present challenge is to extend them to maximize their usefulness until the electrochemical models – and the control-oriented work based on them – 'catch up'. One important phenomenon which has not been adequately explored in the context of state estimation is self-discharge. The work described in this paper describes how this has been approached. In this study, the self-discharge phenomenon is investigated for a new 21 Ah Li-S cell. As a contribution of this study, an equivalent-circuit-network model was developed for the Li-S cell by considering the effect of cell's self-discharge. A system identification approach was used to parameterize the model based on experimental data. The original model was then extended by adding a self-discharge resistance to it. To obtain the self-discharge resistance, a particular new series of experiments were designed and performed on the Li-S cell at various temperature and initial state-of-charge levels.

Li-S Cell ECN Modelling

ECN modelling approach.—There are various approaches of cell modelling in the literature. They can be classified into different categories such as mathematical, electrochemical and electrical circuit methods. A review on different battery modelling approaches is presented in Ref. 16. An electrochemical cell model is the most accurate one however, the complexity of such model usually restricts it to be used on control boards in real-time. Therefore, other Low-fidelity modelling approaches like electrical circuit modelling or equivalent circuit network (ECN) modelling have been proposed to strike a balance between model complexity and accuracy.[17] ECN models have been used in a wide range of applications and various types of batteries.[18–20]

An ECN model simply contains resistors, capacitors and voltage sources which are put together in an electrical circuit. A very common form of an ECN model contains a resistance in series with one RC network as shown in Figure 3 that is called Thevenin model.[21,22] The model contains an ideal voltage source representing the cell's open-circuit voltage (V_{OC}), a resistance representing the cell's ohmic resistance (R_O) and a *RC* network containing polarization resistance (R_P) and polarization capacitance (C_P). As shown in Figure 3, V_t is battery terminal voltage and I_L is the load current.

In Ref. 8 a standard ECN model (like shown in Figure 3) was used in which the parameters of the cell's model are considered as functions

Downloaded on 2018-01-22 to IP 138.250.27.251 address. Redistribution subject to ECS terms of use (see ecsdl.org/site/terms_use) unless CC License in place (see abstract).

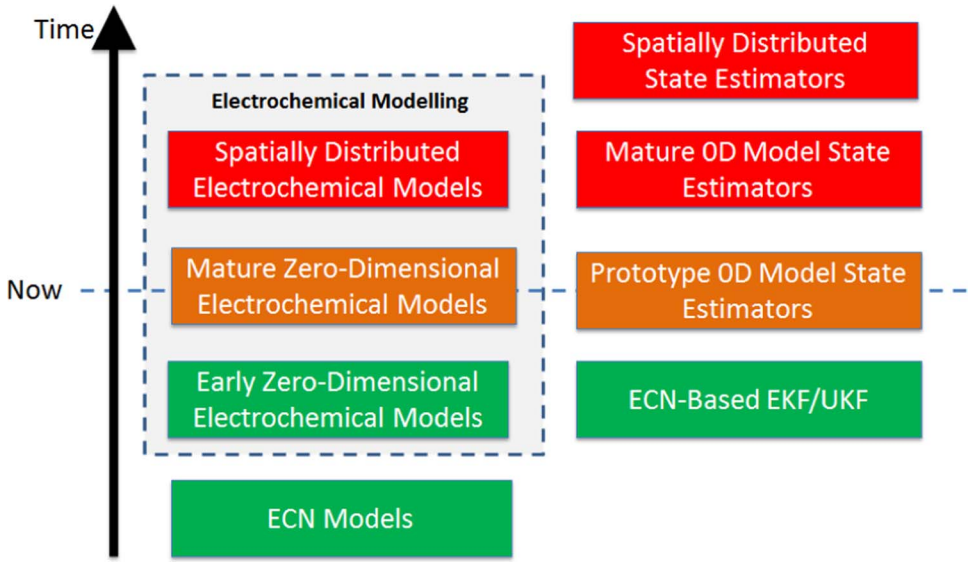


Figure 2. Expected road map for state estimation in Li-S: colors are a 'traffic light' indication of technology readiness, with green representing most ready, and red representing furthest off.[14]

of the cell's SoC (denoted by X). The input to the ECN model is the load current I_L(t), and the output of the model is the cell's terminal voltage $V_t(t)$. So, the output equation can be written in the following form:

$$V_t(t) = h_{V_t}(X,\ V_{RC},\ I_L) = V_{oc}(X) - V_{RC}(X) - R_o(X)\, I_L(t) \quad [5]$$

where V_{RC} is the voltage across the RC network.

This model has two states that can describe its dynamic behavior. These states are state-of-charge (SoC) and the capacitor's voltage denoted by V_{RC}. The following equations show the state derivatives of the model:[8]

$$\dot{X} = f_x(I_L) = -\frac{1}{Q_{\text{cap}}} I_L(t) \quad [6]$$

where Q_{cap} represents the capacity of the battery under consideration in coulombs.

$$\dot{V}_{RC} = f_{\dot{V}_{RC}}(X,\ V_{RC},\ I_L) \quad [7]$$

where

$$f_{\dot{V}_{RC}}(X,\ V_{RC},\ I_L) = -\frac{1}{R_P(X)\, C_P(X)} V_{RC} + \frac{1}{C_P(X)} I_L(t) \quad [8]$$

To facilitate the system identification process (will be described in Model parameterization section), the model is re-parameterized by defining new behavioral variables as follow:

$$\Omega_P(X) = \frac{1}{R_P(X)\ C_P(X)} \quad [9]$$

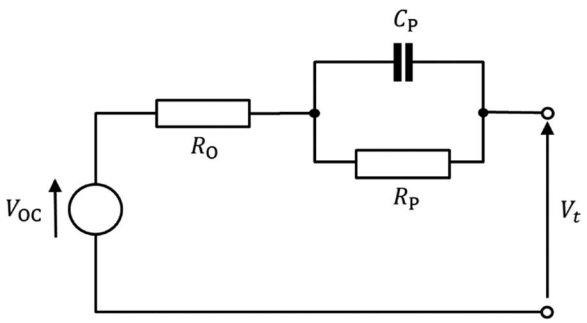


Figure 3. Thevenin battery model.

$$R_{\text{int}}(X) = R_o(X) + R_P(X) \quad [10]$$

$$\rho_P(X) = \frac{R_P(X)}{R_{\text{int}}(X)} \quad [11]$$

where $\Omega_P(X)$ is the dynamic bandwidth defined by R_P and C_P, R_{int} is the total steady-state resistance, which affects the voltage drop when applying continuous discharge current, and ρ_P is the response dynamic fraction.

In such way that when $\rho_P = 0$, the response of the voltage is completely instantaneous, and when $\rho_P = 1$, the response will be dynamic. The implementation of the constraints is much easier when using this behavioral parametrization:

$$\begin{aligned} \Omega_P(X) &\in [\Omega_{\min}, \Omega_{\max}] \\ R_{\text{int}}(X) &> 0 \\ \rho_P(X) &\in [0, 1] \end{aligned} \quad [12]$$

Subsequently, we can re-write the output equation and the states derivative equations based on the new behavioral parametrization as follows:[8]

$$\begin{aligned} V_t(t) = h_{V_t}(X,\ V_{RC},\ I_L) = V_{oc}(X) - V_{RC}(X) \\ -[1 - \rho_P(X)] R_{\text{int}}(X)\, I_L(t) \end{aligned} \quad [13]$$

$$\dot{X} = f_x(I_L) = -\frac{1}{Q_{\text{cap}}} I_L(t) \quad [14]$$

$$f_{\dot{V}_{RC}}(X,\ V_P,\ I_L) = -\Omega_P(X)\ V_{RC} + \rho_P(X)\ R_{\text{int}}(X)\, \Omega_P(X)\ I_L(t) \quad [15]$$

Experimental test on Li-S cell.—The Li-S cell investigated in this study was provided by OXIS Energy[23] with specifications presented in Table I. One of the main advantages of Li-S cells is their higher specific energy. The cell that is used here is a prototype with specific energy of 185 Wh/kg which is less than the final product, expected to have an specific energy more than 400 Wh/kg.[23] A Kepco BOP DC power supply (source and sink) was used for charge and discharge of the cell. The device was programmed to apply a current profile as input and cell's terminal voltage was recorded as output. The temperature was controlled during all experiments by putting the cell inside a

Downloaded on 2018-01-22 to IP 138.250.27.251 address. Redistribution subject to ECS terms of use (see ecsdl.org/site/terms_use) unless CC License in place (see abstract).

Table I. Specifications of Li-S cell.

Type	Rechargeable lithium-sulfur pouch cell Remarks: Li Metal Anode
cell dimension	176 mm × 114 mm × 13.7 mm
maximum voltage	2.45 V
nominal voltage	2.05 V
capacity	21 Ah (at 0.2 C, 30°C)
weight	233 ± 5 g
volume	0.252 L
recommended charging condition in applications	2.1 A constant current (C/10) at 30°C (charge stop at 2.45 V or 11 h max charge time)
recommended discharging condition in applications	peak discharge current: 2 C maximum continuous discharge current (at 30°C): 1.5 C
maximum continuous power	60 W (at 30°C)
optimum operating temperature	30°C

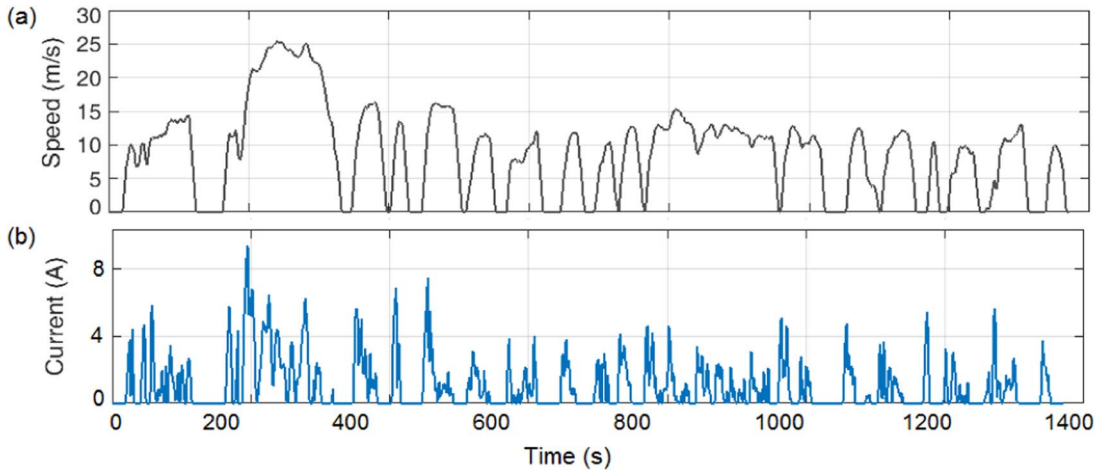


Figure 4. UDDS velocity profile and the scaled current profile.

thermal chamber. The tests started from fully charged state (2.45 V) continuing until the terminal voltage drops below the cut-off voltage (1.5 V) that means depleted state. The measurements include time, current and terminal voltage which are recorded in time domain with a sampling rate of 1 Hz.

Battery testing is possible using different current profiles. Since we were interested in real applications, as a case-study, a current profile was used based on EV power demand on urban dynamometer driving schedule (UDDS) also known as U.S. FTP-72 (Federal Test Procedure).[24] The main feature of such profile is the random change of current value in a realistic scenario. In order to obtain this current profile, a typical EV (i.e. Nissan Leaf) was simulated on UDDS drive cycle as discussed in Ref. 25. The power demand signal was then scaled-down to be applied to the Li-S cell. Since this is a prototype cell, the current was limited below 10 A. This doesn't affect our results and conclusions because the final cells will have same characteristics curves in shape. Figure 4 shows UDDS velocity profile and the corresponding scaled current profile. The current profile was applied to a fully charged cell and it was repeated until the cell became depleted. The cell's terminal voltage subjected to UDDS test is presented in Figure 5. The temperature was controlled at 20°C during this test.

Model parameterization.—In this section, the parameters of the Thevenin model are determined based on the experimental data. For this purpose, a system identification algorithm called Prediction-Error Minimization (PEM)[26] is used. It is demonstrated in Ref. 17 that PEM algorithm is quite suitable for Thevenin battery model parameterization. The identification algorithm determines a vector of unknown parameters (θ) in a way that a prediction error (ε) is minimized as follows:

$$\varepsilon(t_k, \theta) = y(t_k) - \hat{y}(t_k | t_{k-1}; \theta) \quad [16]$$

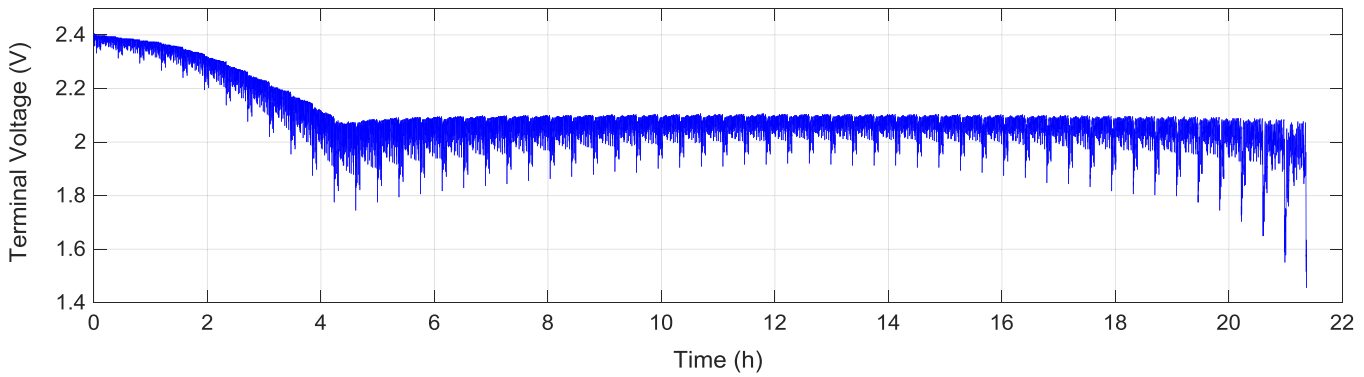


Figure 5. Terminal voltage of Li-S cell subjected to UDDS current profile.

Downloaded on 2018-01-22 to IP 138.250.27.251 address. Redistribution subject to ECS terms of use (see ecsdl.org/site/terms_use) unless CC License in place (see abstract).

where $y(t_k)$ is the measured output at time k and $\hat{y}(t_k|t_{k-1};\theta)$ is the estimated output at time k using the set of parameters θ. So, the prediction error value directly depends on the choice of parameters. In PEM algorithm, a scalar fitness function is minimized as follows:

$$E_N(\theta) = \det\left(\frac{1}{N}\sum_{k=1}^{N}\varepsilon(t_k,\theta)\,\varepsilon^T(t_k,\theta)\right) \quad [17]$$

In case of the Thevenin model, the vector of unknown parameters includes open-circuit voltage (V_{OC}), ohmic resistance (R_O), polarization resistance (R_P) and polarization capacitance (C_P). During the identification process, these parameters are obtained so that the least difference between the measured and estimated values of terminal voltage (V_t) is achieved. So, the vector of unknown parameters and the error function can be presented as follows:

$$\theta = [V_{OC},\ R_O\ ,\ R_P\ ,\ C_P] \quad [18]$$

$$\varepsilon(t_k,\theta) = V_t(t_k) - \hat{V}_t(t_k|\,t_{k-1};\theta) \quad [19]$$

A cell is a highly nonlinear system with time-varying parameters. Therefore, the cell model's parameters need to be updated regularly. The cell's state-of-charge (SoC), state-of-health (SoH) and temperature are factors that can significantly affect the identification result. Temperature is kept constant using the thermal chamber, and SoH variation is out of the scope of this study. However, the effect of SoC variation is considered by repeating the parameterization process at different SoC levels. At each SoC level, a time window (i.e. identification window) of the measurements was used for parameter identification.

Figure 6 presents the parameterization results for the Li-S cell tested in this study. The UDDS test data explained in the previous section was used. PEM algorithm was used to obtain the four unknown parameters of the Thevenin model. The identification window was 5% SoC in this case. As expected, the parameters are nonlinear functions of SoC.

Model validation.—For validating the identification results, the proposed model's output is compared with real measurement data under same condition. Figure 7 shows such a comparison where Li-S cell's terminal voltage is obtained during the UDDS discharge test in two ways: (i) the parameterized Thevenin model and (ii) real measurement. As shown in the figure, there is a good fit between the estimated and measured voltage values.

Li-S Cell Self-Discharge Modelling

Battery self-discharge phenomenon.—The phenomenon of self-discharge is particularly pronounced in Li-S batteries due to the specific properties of the different reaction products during the cycling. The detailed reaction path is complex and still under investigation.[27] When elemental sulfur is reduced, lithium-polysulfides of different length are built. At the beginning of the discharge the majority of reaction products are high order polysulfides (Li2S8 – Li2S6), which are further reduced to lithium sulfide (Li2S) toward the end of discharge. The high-order polysulfides are chemically active and tend to dissolve in common electrolytes. This enables them to be mobile, which means they can move and react to smaller length polysulfides directly with the anode. In charging condition, this effect, called polysulfide shuttle,[28,29] could theoretically continue infinitely when the shorter polysulfides migrate back to the cathode and oxidize again (see Figure 8). However, when no energy is provided, the self-discharge is reduced toward lower SoCs with the decreasing amount of high-order polysulfides in the electrolyte.

Modified ECN model.—In order to extend the ECN model described in ECN modelling approach section to encapsulate the self-discharge behavior of the Li-S cell, we added a resistance element R_{sd} parallel to the power source. From the modified ECN model presented in Figure 9, the output equation is:

$$V_t(t)_{sd} = h_{V_t} = (X,\ V_{RC},\ I_L) = V_{oc}(X) - V_{RC}(X) - [1 - \rho_P(X)]R_{int}(X)\,I_L(t) \quad [20]$$

Also, we can derive the states derivative equations as follow:

$$\dot{X} = f_x(I_L) = -\frac{1}{Q_{cap}}I_L(t) - \frac{1}{Q_{cap}}\frac{V_{oc}(X)}{R_{sd}(X)} \quad [21]$$

Where $\frac{1}{Q_{cap}}\frac{V_{oc}(X)}{R_{sd}}$ is the amount of current drawn from the battery while applying no current demand.

$$f_{\dot{V}_{RC}}(X,\ V_{RC},\ I_L) = -\Omega_P(X)\,V_{RC} + \rho_P(X)\,R_{int}(X)\Omega_P(X)\ I_L(t) \quad [22]$$

In many cases it can be assumed that state-dependant parameters have slight variations which qualify them to be treated as a constant. Thus, the non-linear model can be linearized by defining the operating points as follow:

$$\hat{V}_t(t) = V_t(t) - \bar{V}_t$$

$$\hat{i}_L(t) = I_L(t) - \bar{I}_L$$

$$\hat{X} = X - \bar{X}$$

$$\hat{V}_{RC}(t) = V_{RC}(t) - \bar{V}_{RC} \quad [23]$$

Even though, such terms are not usually used in the formal language of control theory. Since the operating points are consistent we know that:

$$\bar{V}_t = h_{V_t} = (X,\ V_{RC},\ I_L) = V_{oc}(\bar{X}) - \bar{V}_t - [1-\rho_P(\bar{X})]R_{int}(\bar{X})\,\bar{I}_L \quad [24]$$

We could do calculus here, but it is better to go straight to the linearized model using mathematical formulation from Ref. 8. Using this formulation, the output and state equations are as follows:

$$\hat{U}_L = \left[\frac{\partial h_{V_t}}{\partial X}\quad \frac{\partial h_{V_t}}{\partial V_{RC}}\right]\hat{x} + \frac{\partial h_{V_t}}{\partial I_L}\hat{i}_L \quad [25]$$

$$\dot{\hat{x}} = \begin{bmatrix}\frac{\partial f_x}{\partial X} & \frac{\partial f_x}{\partial V_{RC}}\\ \frac{\partial f_{V_{RC}}}{\partial X} & \frac{\partial f_{V_{RC}}}{\partial V_{RC}}\end{bmatrix}\hat{x} + \begin{bmatrix}\frac{\partial f_x}{\partial I_L}\\ \frac{\partial f_{V_{RC}}}{\partial I_L}\end{bmatrix}\hat{i}_L \quad [26]$$

where,

$$\frac{\partial h_{V_t}}{\partial X} = c_{11}$$

$$\frac{\partial h_{V_t}}{\partial V_{RC}} = -1$$

$$\frac{\partial h_{UL}}{\partial I_L} = [1-\rho_P]R_{int}$$

$$\frac{\partial f_x}{\partial X} = \frac{1}{Q_{cap}}\frac{1}{R_{sd}(X)}$$

$$\frac{\partial f_x}{\partial V_{RC}} = 0$$

$$\frac{\partial f_{V_{RC}}}{\partial X} = a_{21}$$

$$\frac{\partial f_{V_{RC}}}{\partial V_{RC}} = -\Omega_P$$

$$\frac{\partial f_x}{\partial I_L} = -\frac{1}{Q_{cap}}$$

$$\frac{\partial f_{V_{RC}}}{\partial I_L} = \rho_P\,R_{int}\Omega_P$$

Downloaded on 2018-01-22 to IP 138.250.27.251 address. Redistribution subject to ECS terms of use (see ecsdl.org/site/terms_use) unless CC License in place (see abstract).

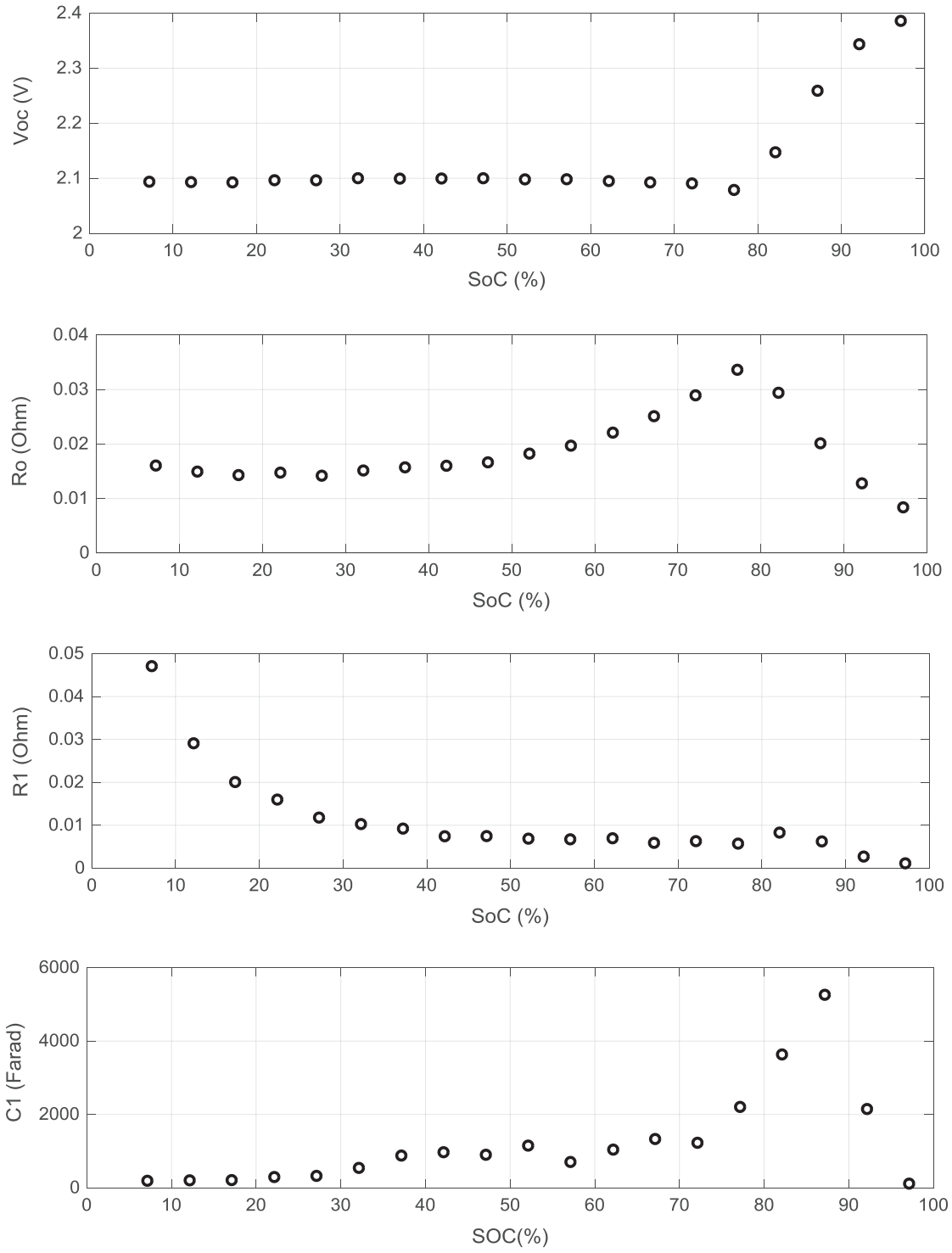


Figure 6. Thevenin model parameterization for a 21 Ah Li-S cell: the four unknown parameters are obtained as a function of SoC.

and then we have:

$$\hat{U}_L = \left[c_{11}\ -1\right]\hat{x}\ +\ \left[1-\ \rho_P\right]R_{\text{int}}\,\hat{i}_L \qquad [27]$$

$$\dot{\hat{x}} = \begin{bmatrix} \frac{1}{Q_{cap}} & \frac{1}{R_{sd}(X)} & 0 \\ a_{21} & & -\Omega_P \end{bmatrix}\hat{x} + \begin{bmatrix} -\frac{1}{Q_{cap}} \\ \rho_P R_{\text{int}}\Omega_P \end{bmatrix}\hat{i}_L \qquad [28]$$

where a_{21} and c_{11} connects the variations in SoC to V_{RC} and V_{RC} respectively.[8] By applying state transformation, the self-discharge model state-space representation becomes as follows.

$$\hat{U}_L = \left[c'_{11}\ -1\right]\hat{z}\ +\ \left[1-\ \rho_P\right]R_{int}\,\hat{i}_L \qquad [29]$$

$$\dot{\hat{z}} = \begin{bmatrix} sd_1 & 0 \\ a'_{21} & -\Omega_P \end{bmatrix}\hat{x} + \begin{bmatrix} -1 \\ \rho_P R_{\text{int}}\Omega_P \end{bmatrix}\hat{i}_L \qquad [30]$$

where sd_1 relates the variations in SoC to self-discharge behavior of the cell.

Downloaded on 2018-01-22 to IP 138.250.27.251 address. Redistribution subject to ECS terms of use (see ecsdl.org/site/terms_use) unless CC License in place (see abstract).

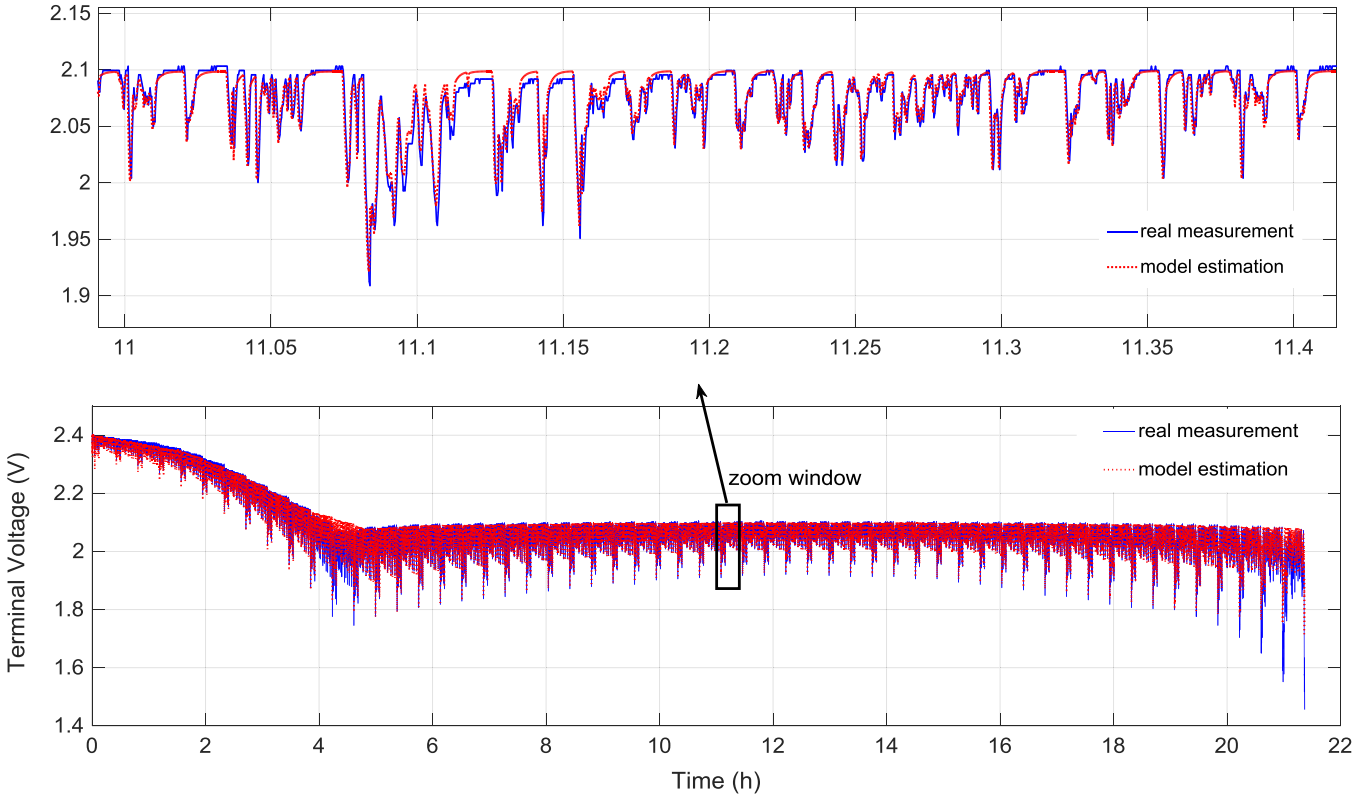


Figure 7. Li-S cell terminal voltage prediction vs. real measurement.

Self-discharge experiment design.—Compared to the transient dynamics, the self-discharge resistance has a slow time constant, so the tests that will quantify it operate over a longer time horizon than the tests used for short-term transient dynamics. The same experimental hardware was used in the self-discharge tests as explained in Experimental test on Li-S cell section. The experimental approach taken here differs as will follow. Knowing that the cell's capacity is 21 Ah, it would take around 10 hours to fully charge/discharge the cell if a constant 2.1 A current is applied to/get from the cell. It was assumed that the energy flow is almost linear during this charge/discharge time. For example, 5 hours charging equivalents to 50% increase in SoC. Thus, the charging time can be used as an indicator of the capacity inside the cell if the initial SoC in known. To have a reference value of the capacity inside the cell, it was assumed that the cell's SoC is around 5–10% when the terminal voltage hits the cut-off voltage limit (1.5 V). The proposed test procedure in this study to investigate Li-S cell's self-discharge phenomenon consists the following 5 steps (steps 2–4 are shown in Figure 10):

Step 1: this is the preparation step. In this step, the cell is subjected to 3 charge/discharge cycles by applying constant current of 0.1 C during both charge and discharge. The limit while charging is reaching the maximum voltage of 2.45 V or maximum charging time of 11 hours whichever occurs first. The extra one hour charging is considered to compensate the power losses assuming a charging efficiency of less than 1. After reaching 100% SoC, the discharge cycle starts by drawing 0.1 C current from the cell until reaching the cut-off voltage (1.5 V). As mentioned before, reaching the cut-off voltage does not mean that the cell is completely depleted (5–10% remaining energy is assumed here).

Step 2: this is the first discharge phase as shown in Figure 10. At this step, the cell is subjected to a constant current demand of 0.1 C until reaching the cut-off voltage.

Step 3: this is the charging step. In this step, the cell is charged with 0.1 C current for a specified number of hours, which will give a nominal state of charge equal to 10% multiplied by the charging time.

Step 4: this is the self-discharge phase in which the cell is left for 24 hours relaxation (zero current). The self-discharge behavior

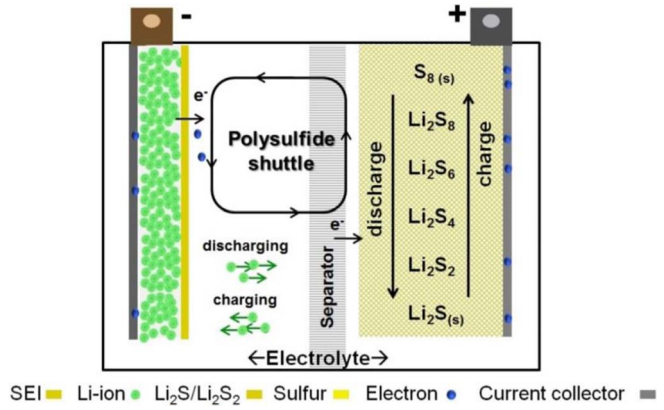


Figure 8. Schematic of polysulfide shuttle in a Li-S cell.

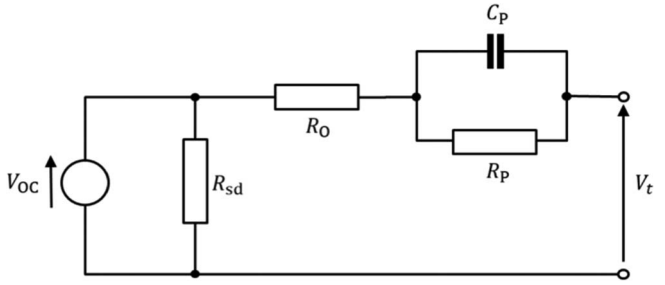


Figure 9. Thevenin battery model with self-discharge resistance.

Downloaded on 2018-01-22 to IP 138.250.27.251 address. Redistribution subject to ECS terms of use (see ecsdl.org/site/terms_use) unless CC License in place (see abstract).

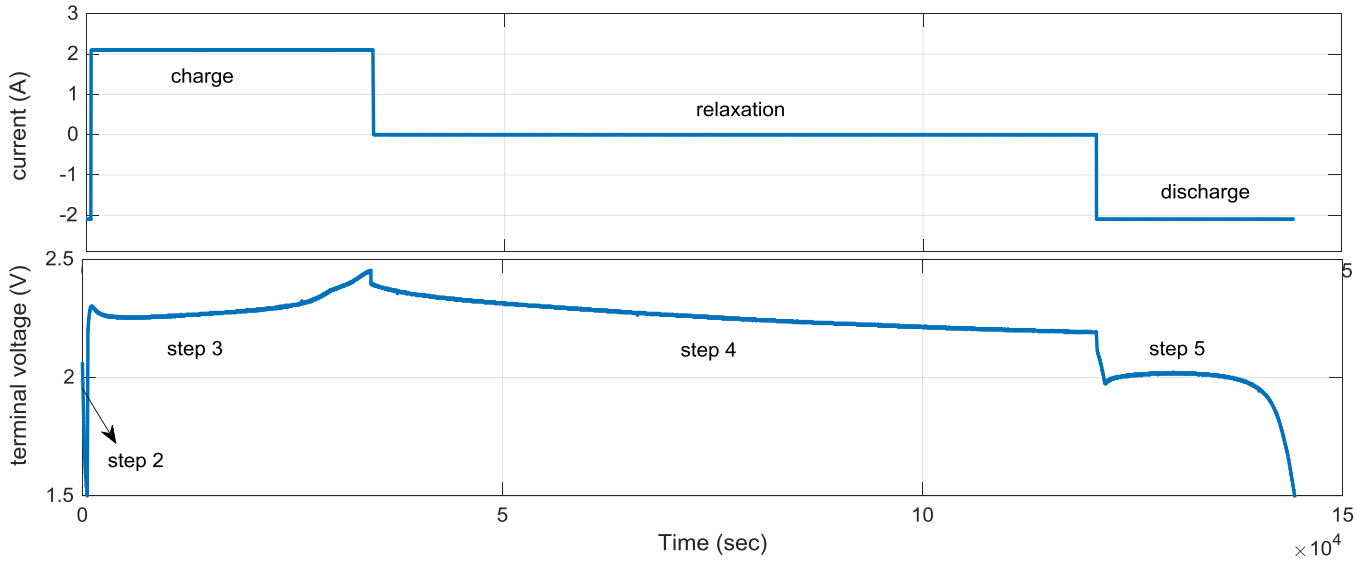


Figure 10. Systematic self-discharge experiment steps.

is assessed based on the OCV measurements. Other relaxation time windows might be considered as well; however, we believe that this time window is enough to capture the average self-discharge resistance value of the cell. It worth noting that because of the cell terminals are connected to the power supply, there was a small current leak from the cell during the relaxation phase (approximately 0.0003 A) – this was treated as a measurement error.

Step 5: this is the second discharge phase as shown in Figure 10. In this step, the remaining capacity inside the cell is obtained. For this purpose, the cell is subjected to 0.1 C constant discharge current until reaching the cut-off voltage again and this is the end of self-discharge experiment.

Calculation of self-discharge resistance (R_{sd}).—In the process described above, to determine the amount of capacity lost due to the cell internal chemistry reactions, the cell was charged at 0.1 C for a specified number of hours, approximately covering the SoC range 10%–100% in 10% increments. The capacity 'lost' due to the internal reactions of the cell for each initial charge level was quantified as follows:

$$\mathrm{Ah_{lost}} = \mathrm{Ah_{charging}} - \mathrm{Ah_{discharging}} \quad [31]$$

where,

$$\mathrm{Ah}_{\mathrm{charging}} = \sum_{j=P_1}^{P_2} I_j$$

$$\mathrm{Ah}_{\mathrm{discharging}} = \sum_{j=P_3}^{P_4} I_j$$

$$\mathrm{A.sec} = I * T_s$$

$$\sum \mathrm{A.sec}_{\mathrm{charging}} = T_1 * T_s * I$$

$$\sum \mathrm{A.sec}_{\mathrm{discharging}} = T_3 * T_s * I$$

$$\mathrm{Ah}_{\mathrm{charging}} = \frac{(T_1 * T_s * I)}{3600}$$

$$\mathrm{Ah}_{\mathrm{discharging}} = \frac{(T_3 * T_s * I)}{3600}$$

where, I represents the charging and discharging current in Ampere, $\mathrm{Ah_{Lost}}$ is the lost capacitance, $\mathrm{Ah_{charging}}$ and $\mathrm{Ah_{discharging}}$ represent the charge and discharge capacitance in Ah, T_s is the measurement sampling time, T_1 and T_3 are charging and discharging time in second, P_1, P_2, P_3 and P_4 represent end point of steps 2, 3, 4, and 5 respectively.

All the necessarily information to calculate the value of an average self-discharge resistance R_{sd} value for each different initial SoC can be obtained from step 4. This is done by firstly calculating an average self-discharge current $I_{\mathrm{sd_average}}$ from the value of the lost capacity as such that

$$I_{\mathrm{sd_average}} = \frac{\mathrm{Ah}_{\mathrm{lost}}}{24} \quad [32]$$

An average OCV is calculated from

$$V_{\mathrm{oc_\ average}} = \frac{\sum_{\mathrm{j=P_3}}^{\mathrm{P_4}} V_{\mathrm{j}}}{N} \quad [33]$$

where,

$$N = 24 * \frac{3600}{T_s}$$

Since we have both $I_{\mathrm{sd_average}}$ and $V_{\mathrm{oc_\ average}}$ the value of $R_{\mathrm{sd_average}}$ can be found from:

$$R_{\mathrm{sd_average}} = \frac{V_{\mathrm{oc_\ average}}}{I_{\mathrm{sd_average}}} \quad [34]$$

Li-S cell self-discharge test results analysis.—Figure 11 presents the capacity loss (Ah) due to self-discharge under different conditions. Ten initial charge levels, and two temperature levels, 10°C and 20°C, were investigated here following the procedure in Calculation of self-discharge resistance (R_{sd}) section.

There are some uncertainties that are worth highlighting. Firstly, although the charging levels nominally correspond to 10% increments in initial state of charge, defining 'full depletion' as the point at which the manufacturer-specified cut-off voltage is reached has limitations. (There is an 'ohmic drop' in the terminal voltage, and the open-circuit voltage usually recovers slightly.) Variations in the system dynamics

Downloaded on 2018-01-22 to IP 138.250.27.251 address. Redistribution subject to ECS terms of use (see ecsdl.org/site/terms_use) unless CC License in place (see abstract).

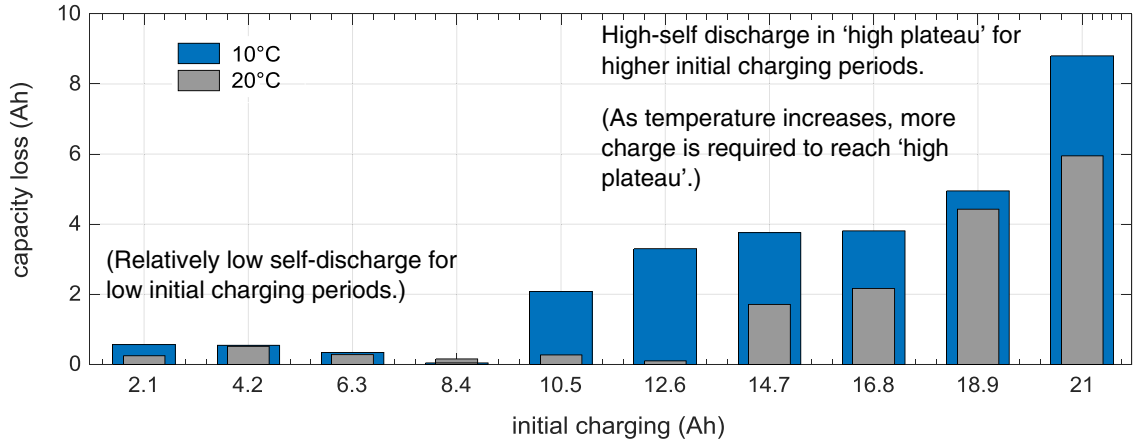


Figure 11. Capacity loss of a 21 Ah Li-S cell due to self-discharge during 24 hours.

may also have an impact. In normal use, the end-point of charging is defined by a voltage level so even with uncertainty about cell capacity or inaccuracies in supply current will not matter: however this can only be done for a 100% initial SoC, and the 'coulomb counting' process used to estimate intermediate SoC levels are likely to be less reliable. In this work, it has been assumed that at cut-off voltage, between 5 and 10% of the SoC remains in the battery: this corresponds to an uncertainty of 1–2 Ah in any estimates of initial state of charge. It is also known that there are complex electrochemical dynamics within a Li-S cell,[13] so it is possible that the reaction pathways 'seen' by a cell initially charged to '80%' then discharged may be different from those encountered in during the 80%–0% region of a full discharge.

In consequence, it should be appreciated that there is a certain degree of uncertainty in these results. This is not likely to be a significant barrier to use in an ECN-based estimator where uncertainty and model error are expected and designed for. However, caution should be taken before drawing strong conclusions about the underlying physics, particularly where 'small' values are involved – small numbers are proportionately more affected by absolute errors.

A first clear outcome from Figure 11 is the dependency of self-discharge rate on the charge level. This result is according to what was reported in Ref. 7 where the Li-S cell's self-discharge becomes more intense as SoC increases. The results also demonstrate that there is a breakpoint at a certain SoC value at which the effect of self-discharge becomes negligible and the trend continues after that. This breakpoint is caused by a significant change in the electrochemical reactions taking place inside a Li-S cell that divide the SoC range into two parts: low and high plateaus.[10] Determination of the exact location of this breakpoint is not simple since it is affected by different factors such as temperature, discharge rate, cell ageing, etc. In addition to these nonlinear affecting parameters, we should add the uncertainty in our calculation of the initial SoC. From Figure 11, such a breakpoint is seen around 50% to 70% (determination of the exact location of the breakpoint is possible using other techniques as discussed in Ref. 10). Furthermore, the relationship between the self-discharge intensity and the SoC level seems linear at high SoC region (high plateau). On the other hand, at the low plateau region, the capacity lost is almost constant and negligible. At 20°C all the 'capacity lost' values are close to zero in the low plateau (below 70% nominal SOC). The small fluctuations in the range of 10%–60% are unlikely to have a scientific meaning as they are likely to be consistent with the uncertainties discussed above.

When comparing outcomes at the two different temperature levels, 10°C and 20°C similar trends are observed, but two new outcomes are seen.: (i) the location of the breakpoint (between high and low plateaus) is shifted to the left (a lower nominal SoC) as temperature decreases, and (ii) the rate of self-discharge appears higher at the lower temperature (i.e. 10°C). In respect of the first observation, it is unlikely that we are seeing significant self-discharge in the low plateau: it is more likely that we see what we do because the Li-S cells' capacity is lower at low temperatures, and the onset of the high plateau therefore occurs earlier during charging at lower temperatures. In respect of the second observation, the Li-S cells' tendency for higher self-discharge at lower temperature is the opposite of what would be expected in lithium-ion cells where self-discharge increases as temperature increases.[30,31] (Another difference between self-discharge in Li-S and Li-ion cells is that Li-ion cells do not usually have significant problems with self-discharge in a short time like one day which is useful in automotive applications.)

Table II contains the self-discharge resistance values (R_{sd}) at different initial charge and temperature levels. These numbers can be used in the proposed ECN model shown in Figure 9. Since there was an uncertainty in calculation of the SoC when hitting the cut-off voltage, small fluctuations of the capacity loss were neglected in this study. Consequently, the self-discharge effect at low plateau is considered almost constant. A resistance value of 100 ohm is equivalent to 0.5 Ah capacity loss at low plateau. On the other hand, the exact values are obtained and used at high plateau as presented in. Table II.

For the Li-S cell investigated in this study, the authors' recommendation would be to store cells at 60% SoC or lower when they will not be used for roughly a day or more. This will help minimize the capacity loss due to the self-discharge effect.

Conclusions

In this study, the self-discharge effect in a Li-S cell was analyzed using a novel quantitative approach. Particular experiments were designed and performed on a 21 Ah Li-S cell and a system identification technique was used to parameterize an ECN model for the cell by considering the self-discharge effect for the first time. Ten initial charge

Table II. Self-discharge resistance values at different initial charge and temperature levels.

initial charge (Ah)	R_{sd} (ohm) at 10°C	R_{sd} (ohm) at 20°C
2.1	100	100
4.2	100	100
6.3	100	100
8.4	100	100
10.5	25.50	100
12.6	16.18	100
14.7	14.30	22.64
16.8	14.18	18.00
18.9	10.97	9.83
21	6.15	7.827

Downloaded on 2018-01-22 to IP 138.250.27.251 address. Redistribution subject to ECS terms of use (see ecsdl.org/site/terms_use) unless CC License in place (see abstract).

levels and two temperature levels, 10°C and 20°C, were investigated. The results show that the Li-S cell's self-discharge becomes more intense as SoC increases. The results also demonstrate that there is a breakpoint at a certain SoC value at which the effect of self-discharge becomes negligible and this trend continues after that. Consequently, a constant self-discharge resistance value of 100 ohm was used at low plateau. The whole tests were repeated at the two temperature levels getting two outcomes: (i) the location of the breakpoint between the high and low plateaus is shifted to the left (lower SoC) as temperature decreases, and (ii) the rate of self-discharge is higher at the lower temperature against the li-ion cells where self-discharge increases as temperature increases.

Acknowledgments

The authors thank OXIS Energy and V. Knap of Aalborg University, Denmark for their help and support. This research was partly undertaken within the Revolutionary Electric Vehicle Battery (REVB) project funded by EPSRC under grant number EP/L505286/1. The underlying data can be accessed through the Cranfield University data repository at https://dx.doi.org/10.17862/cranfield.rd.c.3858703.

References

1. K. J. Aström and R. M. Murray, *Feedback Systems: An Introduction for Scientists and Engineers*, Princeton University Press (2008).
2. G. Vinnicombe, *Uncertainty and Feedback: H∞ Loop-Shaping and the υ -Gap Metric*, Imperial College Press, London (2000).
3. R. E. Kalman, "A New Approach to Linear Filtering and Prediction Problems," *Trans. AMSE – J. Basic Eng.*, **82** (Series D): 35 (1960).
4. G. L. Plett, "Extended Kalman filtering for battery management systems of LiPB-based HEV battery packs – Part 1. Background," *J. Power Sources*, **134**(2), 252 (2004).
5. G. L. Plett, "Extended Kalman filtering for battery management systems of LiPB-based HEV battery packs – Part 1. Background," *J. Power Sources*, **134**(2), 252 (2004).
6. G. L. Plett, "Extended Kalman filtering for battery management systems of LiPB-based HEV battery packs – Part 1. Background," *J. Power Sources*, **134**(2), 252 (2004).
7. V. Knap, D. Stroe, M. Swierczynski, R. Teodorescu, and E. Schaltz, "Investigation of the Self-Discharge Behavior of Lithium-Sulfur Batteries," *J. Electrochemical Society*, **163**(6), A911 (2016).
8. K. Propp, M. Marinescu, D. Auger, L. O'Neill, A. Fotouhi, K. Somasundaram, G. Offer, G. Minton, S. Longo, M. Wild, and V. Knap, "Multi-temperature state-dependent equivalent circuit discharge model for lithium-sulfur batteries," *J. Power Sources*, **328**, 289 (2016).
9. A. Fotouhi, D. J. Auger, K. Propp, and S. Longo, "Electric Vehicle Battery Parameter Identification and SOC Observability Analysis: NiMH and Li-S Case Studies," *IET Power Electronics*, (2017).
10. A. Fotouhi, D. J. Auger, K. Propp, S. Longo, R. Purkayastha, L. O'Neill, and S. Walus, "Lithium-Sulfur Cell Equivalent Circuit Network Model Parameterization and Sensitivity Analysis," *IEEE Transactions on Vehicular Technology*, **66**(9), 7711 (2017).
11. K. Propp, D. J. Auger, A. Fotouhi, S. Longo, and V. Knap, "Kalman-variant estimators for state of charge in lithium-sulfur batteries," *Journal of Power Sources*, **343**, 254 (2017).
12. A. Fotouhi, D. J. Auger, K. Propp, and S. Longo, "Lithium-Sulfur Battery State-of-Charge Observability Analysis and Estimation," accepted for publication in *IEEE Transactions of Power Electronics* ,(2017).
13. M. Marinescu, T. Zhang, and G. J. Offer, "A zero dimensional model of lithium–sulfur batteries during charge and discharge," *Phys. Chem. Chem. Phys.*, **18**, 584 (2016).
14. D. J. Auger, "Using ideas from control theory in the modelling and management of lithium-sulfur batteries," (lecture, University of Oxford, February 6, 2017).
15. A. M. Bizeray, S. Zhao, S. R. Duncan, and D. A. Howey, "Lithium-ion battery thermal-electrochemical model-based state estimation using orthogonal collocation and a modified extended Kalman filter," *J. Power Sources*, **296**, 400 (2015).
16. A. Fotouhi, D. J. Auger, K. Propp, S. Longo, and M. Wild, "A review on electric vehicle battery modelling: From Lithium-ion toward Lithium–Sulphur," *Renewable and Sustainable Energy Reviews*, **56**, 1008 (2016).
17. A. Fotouhi, D. J. Auger, K. Propp, and S. Longo, "Accuracy Versus Simplicity in Online Battery Model Identification," *IEEE Transactions on Systems, Man, and Cybernetics: Systems*, PP(99): 1 (2017).
18. T. Marc, B. Oliver, and U. S. Dirk, "Development of a voltage-behavior model for NiMH batteries using an impedance-based modeling concept," *J. Power Sources*, **175**, 635 (2008).
19. A. Fotouhi, D. J. Auger, K. Propp, and S. Longo, "Electric Vehicle Battery Parameter Identification and SOC Observability Analysis: NiMH and Li-S Case Studies," *IET Power Electronics*, (2017).
20. H. He, R. Xiong, and J. Fan, "Evaluation of Lithium-Ion Battery Equivalent Circuit Models for State of Charge Estimation by an Experimental Approach," *Energies*, **4:** 582 (2011).
21. L. Thevenin, "Extension of Ohm's law to complex electromotive circuits," in: *Ann. Telegr.*, **3**(10), 222.
22. L. Thevenin, *CR Seances l'Academie Sci*, **9**, 159 (1883).
23. OXIS Energy (company web site), http://www.oxisenergy.com, accessed August 21, 2017.
24. Emissions Cycles: FTP-72 (UDDS), DieselNet (website), https://www.dieselnet.com/standards/cycles/ftp72.php, accessed August 21, 2017.
25. A. Fotouhi, N. Shateri, D. J. Auger, S. Longo, K. Propp, R. Purkayastha, and M. Wild, "MATLAB graphical user interface for battery design and simulation; from cell test data to real-world automotive simulation," SMACD2016, Lisbon.
26. L. Ljung, *System Identification - Theory for the User*, Prentice Hall, New York (1987).
27. M. Wild, L. O'Neill, T. Zhang, R. Purkayastha, G. Minton, M. Marinescu, and G. J. Offer, "Lithium sulfur batteries, a mechanistic review," *Energy & Environmental Science*, **8** (12), 3477 (2015).
28. Y. V. Mikhaylik and J. R. Akridge, "Polysulfide shuttle study in the Li/S battery system," *J. Electrochem. Soc.*, **151**(11): A1969 (2004).
29. D. Moy, A. Manivannan, and S. R. Narayanan, "Direct measurement of Polysulfide shuttle current; a window into understanding the performance of lithium-sulfur cells," *J. Electrochem. Soc.*, **162**(1): A1 (2015).
30. G. M. Ehrlich, *Handbook of Batteries*, 3rd ed., D. Linden and T. B. Reddy, Editors, p. 35.1, McGraw-Hill, New York (2002).
31. B. A. Johnson and R. E. White, "Characterization of commercially available lithium-ion batteries," *J. Power Sources*, **70:** 48 (1998).

Downloaded on 2018-01-22 to IP 138.250.27.251 address. Redistribution subject to ECS terms of use (see ecsdl.org/site/terms_use) unless CC License in place (see abstract).



https://dspace.org/

Self-discharge effects in lithium-sulfur equivalent circuit networks for state estimation

Yousif, S. E. A.; Fotouhi, Abbas; Auger, Daniel J.; Propp, Karsten

2017-11-30
Electrochemical Society
http://dx.doi.org/10.1149/2.0121801jes
S. E. A. Yousif, A Fououhi, D. J. Auger and K Propp. Self-discharge effects in lithium-sulfur equivalent circuit networks for state estimation. Journal of The Electrochemical Society, 2018, Volume 165, Issue 1, A6081-A6090

Downloaded from a DSpace repository. https://dspace.org/